Chinese Chemical Letters 35 (2024) 110176

Contents lists available at ScienceDirect

Chinese Chemical Letters

journal homepage: www.elsevier.com/locate/cclet

Constructing the synergistic active sites of nickel bicarbonate supported Pt hierarchical nanostructure for efficient hydrogen evolution reaction

Weiping Xiao[a,b,*], Yuhang Chen[a], Qin Zhao[a], Danil Bukhvalov[a], Caiqin Wang[a], Xiaofei Yang[a,*]

[a] College of Science, Institute of Materials Physics and Chemistry, Nanjing Forestry University, Nanjing 210037, China
[b] Key Laboratory of Advanced Energy Materials Chemistry (Ministry of Education), College of Chemistry, Nankai University, Tianjin 300071, China

ARTICLE INFO

Article history:
Received 25 January 2024
Revised 28 May 2024
Accepted 25 June 2024
Available online 25 June 2024

Keywords:
Hydrogen evolution reaction
Density functional theory
Synergistic active sites
Pt-supported hierarchical nanostructure
Electrocatalysis

ABSTRACT

Constructing synergistic active sites and optimizing the cooperative adsorption energies for hydrogen and hydroxyl based intermediates are two essential strategies to improve the sluggish kinetics of hydrogen evolution reaction (HER) in alkaline medium. However, it is still in its infancy to simultaneously achieve these goals, especially for designing a well-defined carrier with multiple hydroxyl adsorption sites. Herein, the $Ni(HCO_3)_2$ nanoplates (NHC) with horizontal interfaces sites of Ni-terminated NiO, NiOOH, NiCOO, and $Ni(OH)_2$ were employed as the hydroxyl adsorption active sites, which could anchor Pt particles with hydrogen adsorption active sites, constructing the synergistic active sites (NHC-Pt) for HER catalysis. Evidenced by X-ray photoelectron spectroscopy (XPS) and extended X-ray absorption fine structure (EXAFS), the NHC could affect the chemical state and electronic structure of Pt particles by forming bond of Pt-O which could reduce the reaction energy barriers, facilitate the adsorption of hydrogen and establishment of H–H bond. Furthermore, density functional theory (DFT) theoretical calculation revealed that the related process of hydroxide was the rate-determining step. It is demonstrated the hydroxyl group presents the lowest energy barrier for desorption in the process of HER when the gradual desorption process could be described as a migration from $Ni(HCO_3)_2$·OH directly or *via* other Ni-based systems formed after partial decomposition of nickel hydrocarbonate to $Ni(OH)_2$···OH with following desorption. As a result, the NHC-Pt hierarchical nanostructure demonstrated superior activity towards HER in a pH-universal solution. This enhancement can be attributed to the optimized electronic structure of Pt, the migration of hydroxyl group on NHC substrates, and the synergistic effects between the NHC carrier and Pt particles.

Hydrogen, as a clean energy carrier for fuel cells, has aroused great attention for its reproducibility and zero-carbon emission. The electrocatalytic hydrogen evolution reaction (HER) from water splitting is a crucial method for obtaining hydrogen energy. However, it often involves complex reaction pathways, presents additional energy barriers, and consequently exhibits sluggish reaction kinetics [1–5]. To enhance the kinetics, the catalysts are essential and the mechanism of the HER is needed to be understood. In acidic medium, the reaction ($2H^+ \rightarrow H_2$) is straightforward and verified by Sabatier's principle and Butler-Volmer equation. The binding energies of hydrogen at the active sites on the catalyst surface are responsible for the HER activities. The catalysts, such as Pt and Ir, with moderate hydrogen adsorption strength (ΔG_{H^*} close to 0 V) could, consequently, give rise to the optimal catalytic HER activity [6–9]. On the contrary, in alkaline medium, it is still debatable why the reaction kinetics of the catalysts including Pt-group metals are two to three orders of magnitude slower and more sensitive to the catalysts' surface structure than in acid solution [10,11]. Numerous studies have reported the existence of volcano-shaped curves correlating HER activities with the binding energy of hydrogen in alkaline media. This observation, in accordance with Sabatier's principle, suggests the presence of an optimal binding energy for hydrogen [12–15]. Research regarding the HER/HOR activities of Pt-group metal catalysts has shown that these activities are primarily influenced by the binding energy of hydrogen and are minimally correlated to the adsorption of hydroxide. Accordingly, to enhance

* Corresponding authors.
E-mail addresses: wpxiao@njfu.edu.cn (W. Xiao), xiaofei.yang@njfu.edu.cn (X. Yang).

https://doi.org/10.1016/j.cclet.2024.110176
1001-8417/

the HER performance of Pt-based materials, alloy methods have been adopted to optimize the binding energy of hydrogen, and under the circumstances, the second metal such as Ru is underneath rather than on the Pt surface [16,17]. The second metal, such as Ru or Ni, on the surface could promote the adsorption of hydroxide but the enhanced performance can hardly be explained as an oxyphilic effect [18–20].

However, an increasing number of experimental and theoretical research papers have indicated that the adsorption of hydroxide also affects the HER kinetics [21–23]. This requires the second active site to adsorb hydroxide and promotes H_2O dissociation, which consequently enhances the HER kinetics [24]. The alkaline HER/HOR activities of Pt-Ru alloy catalysts were much higher than the commercial Pt/C, which was partly due to the stronger adsorption of hydroxide [25]. This alloy metal makes it still uncertain how the second metal affects the HER kinetics of Pt-based compound from the theoretical research since the binding energy of hydroxide is untoward to calculation by density functional theory. Moreover, Pt-metal supported composites are increasingly gaining attention in research as potential substitutes for alloying catalysts [26]. This is due to their advantages such as high utilization of noble metal atoms and robust Pt-support interactions. The support material can not only disperse and anchor Pt particles to enhance the stability but also can serve as active sites for hydroxyl species adsorption. These synergistic active sites can concurrently increase catalytic activity and stability. For example, $Ni(OH)_2$-Pt manifests an enhancement of HER performance relative to state-of-the-art Pt catalyst, ascribing to the $Ni(OH)_2$ nanoparticles on Pt electrode surfaces could induce the dissociation of H_2O [23]. Hence, by constructing Pt supported hierarchical nanostructure based on bi-functional mechanism, the Pt and carriers have synergistic active sites to adsorb the species of hydrogen and hydroxyl, respectively, which facilitate to the break of O–H in H_2O molecules, and could simultaneously boost catalytic activity and stability. However, most of the research is focused on the development of supports with single active site. Compared with single active site, the multiple active sites could exhibit various adsorption strengths of hydroxyl group and it may bring further improvement to the electrocatalytic performance.

Based on the above analysis, the synergistic active sites were constructed to regulate the migration of intermediate species in the process of HER in alkaline solution. The support with the ability to adsorb the hydroxide were employed as $Ni(HCO_3)_2$ (namely NHC) nanoplates, which includes interfacial sites of Ni-terminated NiO, NiOOH, NiCOO, and $Ni(OH)_2$. When compounding Pt with NHC to forming NHC-Pt, Pt could act as the hydrogen adsorption active sites and obtain the synergistic active sites for HER catalysis. The uniformly distributed NHC nanoplates could provide an ideal platform for Pt nanoparticles (NPs) to be uniformly dispersed, making sure that the maximum exposure of active sites. The NHC-Pt hierarchical nanostructure exhibits enhanced electrochemical active surface area and preferable activities toward HER in pH-universal solution, which could be originated from the synergistic effect between the NHC carrier and Pt nanoparticles. The density functional theory (DFT) based simulations have been carried out to reveal the pathways and energetics of performed reactions. This tendency found in our modeling provides the possibility for further guiding the design of Pt hierarchical nanostructure with synergistic active sites for HER in alkaline media.

The NHC-Pt-3 compound was prepared by anchoring Pt-based nanoparticles to NHC nanoplates *via* a facile two-step method. In detail, two-dimensional NHC nanoplates were firstly synthesized by a simple solvothermal reaction, which was used as a template to load and disperse the Pt nanoparticles. The synthesized NHC and H_2PtCl_6 solution were dispersed in ethylene glycol solution maintaining at 120 °C for 2 h under oil bath which resulted in the Pt nanoparticles *in-situ* grown on NHC nanoplates, defined as NHC-Pt. By adjusting the mass ratio of Pt and NHC-Pt to 1%, 2%, 3%, 5%, the NHC-Pt-1, NHC-Pt-2, NHC-Pt-3, NHC-Pt-5 were prepared, respectively.

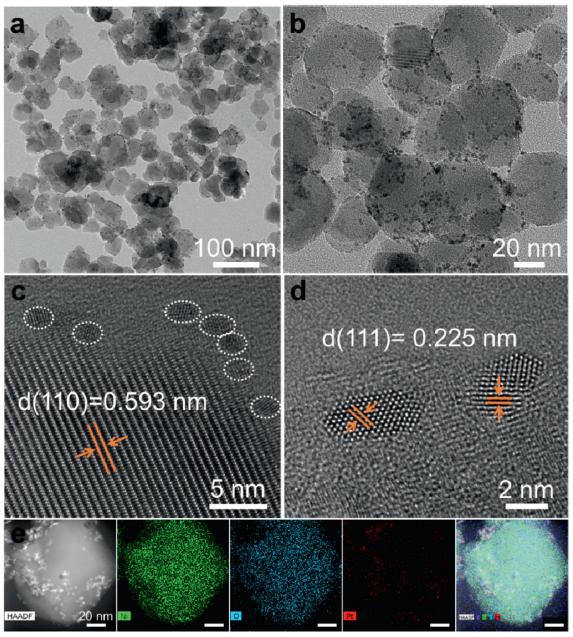

Fig. 1. Structural characterization. TEM image of NHC-Pt-3 at the scale bar of (a) 100 nm and (b) 20 nm. (c, d) HAADF-TEM images of NHC-Pt-3 nanomaterials. (e) HAADF-STEM image and the corresponding EDS elemental mapping of NHC-Pt-3.

Transmission electron microscopy (TEM) image of NHC-Pt-3 showed the obtained nanoplates distributed isolated with a diameter of 31−49 nm (Fig. 1a, Figs. S1 and S2 in Supporting information). Furthermore, AFM measurement indicated that the average thickness of the $Ni(HCO_3)_2$ nanosheets was ~13 nm (Fig. S3 in Supporting information). The Pt nanoparticles were evenly distributed on the nanoplates, with sizes ranging from 1 nm to 3 nm (Fig. 1b, Figs. S4 and S5 Supporting information). This distribution suggests that the NHC could mitigate the aggregation of Pt nanoparticles to some extent. High-angle annular dark-field transmission electron microscopy (HAADF-TEM) showed the lattice fringes of NHC and Pt. The interplanar spacing was calculated to be 0.593 nm, corresponding to the (110) crystal face of NHC (Fig. 1c). While the lattice spacing of 0.225 nm was relevant to the (111) crystal face of Pt nanoparticles (Fig. 1d). The HAADF-STEM image and the corresponding EDS elemental mapping of NHC-Pt-3 confirms that the Ni, O elements were well distributed throughout the nanoplate while the Pt atoms are scattered dispersed on the $Ni(HCO_3)_2$ nanoplates, indicating the loading of Pt was relatively low (Fig. 1e). The X-ray diffraction (XRD) patterns give further evidence for the small particles of Pt for the absent characteristic peaks of Pt (Fig. S6 in Supporting information). The inductively-coupled plasma mass spectroscopy (ICP-MS) was carried out as shown in Table S1 (Supporting information) and the weight percent of Pt for NHC-Pt-3 is 15.2%.

The chemical states and surface electronic structure of NHC-Pt-3 were analyzed by X-ray photoelectron spectroscopy (XPS) and compared with NHC and Pt/C. The XPS spectrum of Ni $2p_{3/2}$ peaks for NHC-Pt-3 are located at 855.96 eV and 857.46 eV, ascribing to the Ni^{2+} and Ni^{3+} of Ni 2p (Fig. 2a) [27]. The high resolution XPS Pt 4f spectrum of NHC-Pt-3 was shown in Fig. 2b and it displayed two pairs of peaks located at 70.92/74.32 eV and 72.01/75.71 eV, corresponding to the metallic Pt^0 ($4f_{7/2}/4f_{5/2}$) and Pt^{2+} ($4f_{7/2}/4f_{5/2}$) [27]. The binding energies of Pt 4f on the NHC-Pt-3 catalyst is no-

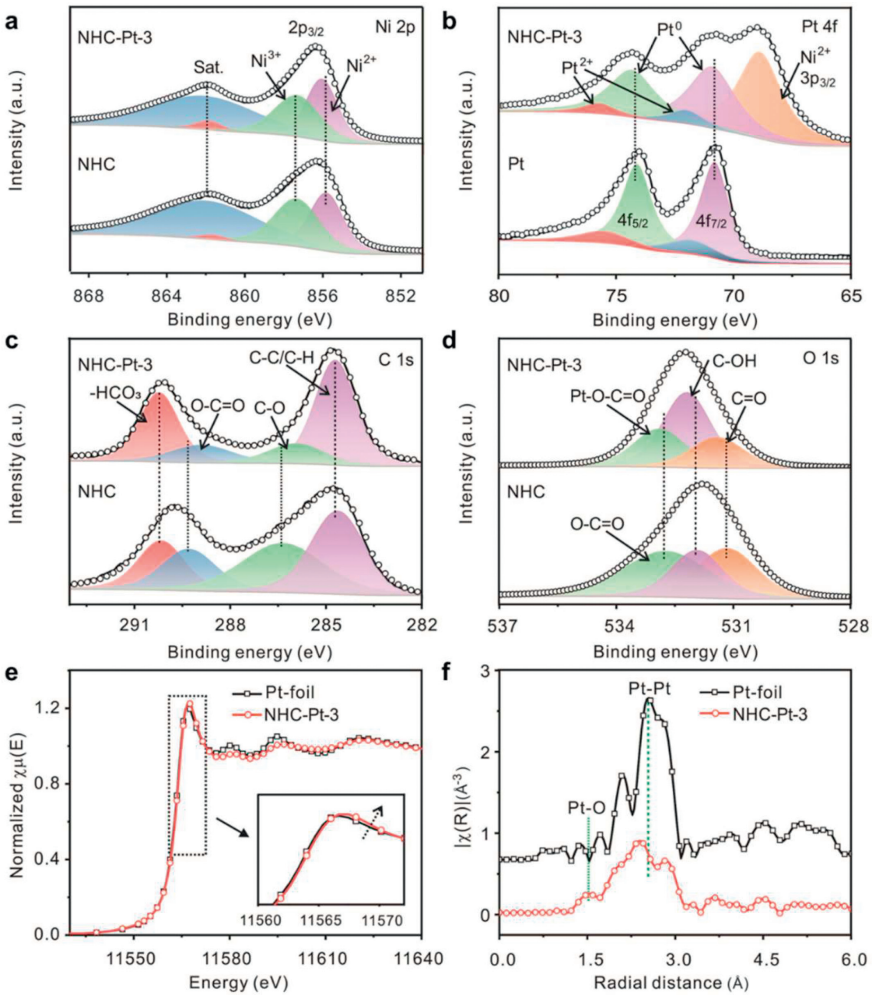

Fig. 2. The XPS spectra of (a) Ni 2p, (b) Pt 4f, (c) C 1s and (d) O 1s on the surface of NHC-Pt-3 and NHC or Pt/C. Pt L-edge (e) XANES spectra and (f) EXAFS spectra of Pt foil and NHC-Pt-3, respectively.

tably higher than that of the Pt/C catalyst. This indicates a downshift of the d-band center of Pt and a robust electronic interaction between the NHC and Pt atoms. Such interactions could lower the hydrogen binding energy and promote the kinetics of hydrogen evolution reaction [28]. The another peak at 68.8 eV was assigned to Ni^{2+} 3p of $Ni(HCO_3)_2$ [29]. The C 1s spectrum of NHC-Pt-3 catalyst showed four peaks at 290.15, 288.88, 285.95 and 284.80 eV, corresponding to the $-HCO_3$, O–C=O, C–O and C–C/C–H, respectively [30,31]. The binding energy of O–C=O, C–O shifted to negative position for 0.23 eV and 0.35 eV relative to the pristine NHC (Fig. 2c). Meanwhile, the O 1s peak for O–C=O shifted to higher binding energy after compositing NHC with Pt, providing further evidence for the formation of Pt–O–C=O and electronic transform from Pt to NHC (Fig. 2d) [32,33]. The X-ray absorption near-edge structure (XANES) and extended X-ray absorption fine structure (EXAFS) were conducted and the results were analyzed to in-depth understanding the chemical states and bonding situation of Pt before and after combination with NHC carrier. Fig. 2e compared the Pt L-edge XANES of NHC-Pt-3 and Pt-foil. It could be seen that the XANES edge data of NHC-Pt-3 presented a higher energy shift relative to Pt-foil, indicating the existence of higher oxidation state of Pt and the electrons transform from Pt to NHC in NHC-Pt-3 compound [34]. This phenomenon is in accordance with the XPS analysis that the binding energy of Pt shifts positive after accord with NHC. Fig. 2f displayed the Pt L-edge EXAFS of NHC-Pt-3 and Pt-foil. The peak position located at 2.5 Å in Pt-foil are corresponding to the Pt-Pt bonding, which shifted to the lower value and weaker intensity in NHC-Pt-3 compound, suggesting the bond strength of Pt-Pt coordination is weaker in NHC-Pt-3 compared with that in Pt-foil [35]. The NHC-Pt-3 compound also showed a peak at 1.6 Å corresponding to Pt-O coordination [36,37], absent in the curve of Pt-foil, indicating the bonding of Pt and O and strong interaction between Pt and NHC. This could regulate the chemical state and electronic structure of Pt, thereby decrease the hydrogen binding energy and further optimize the HER catalytic activity of the NHC-Pt [32].

The electrocatalytic performances toward HER of the NHC, NHC-Pt-1, NHC-Pt-2, NHC-Pt-3 and NHC-Pt-5 samples were evaluated and compared in 1 mol/L KOH, 1 mol/L PBS and 0.5 mol/L H_2SO_4 solution. The linear sweep voltammetry (LSV) curves of different catalysts were conducted from 0.1 V to −0.5 V at 5 mV/s in 1 mol/L KOH aqueous solution (Fig. 3a). The current densities of different samples were enhanced with the increase of overpotential. The current density enhanced gradually for NHC samples while it increased dramatically for NHC-Pt compound samples. The NHC-Pt-1, NHC-Pt-2, NHC-Pt-3 and NHC-Pt-5 required an overpotential of 289 mV, 121 mV, 51 mV and 37 mV to obtain a current density of 10 mA/cm^2, indicating the HER activities were enhanced with the increasing of the Pt loading. The overpotential of NHC-Pt-2, Pt-3 and NHC-Pt-5 are much smaller than that of Pt/C (122 mV). The corresponding Tafel slopes of NHC, NHC-Pt-1, NHC-Pt-2, NHC-Pt-3 and NHC-Pt-5 achieves 1194.3, 117.6, 66.0, 37.2 and 30.6 mV/dec,

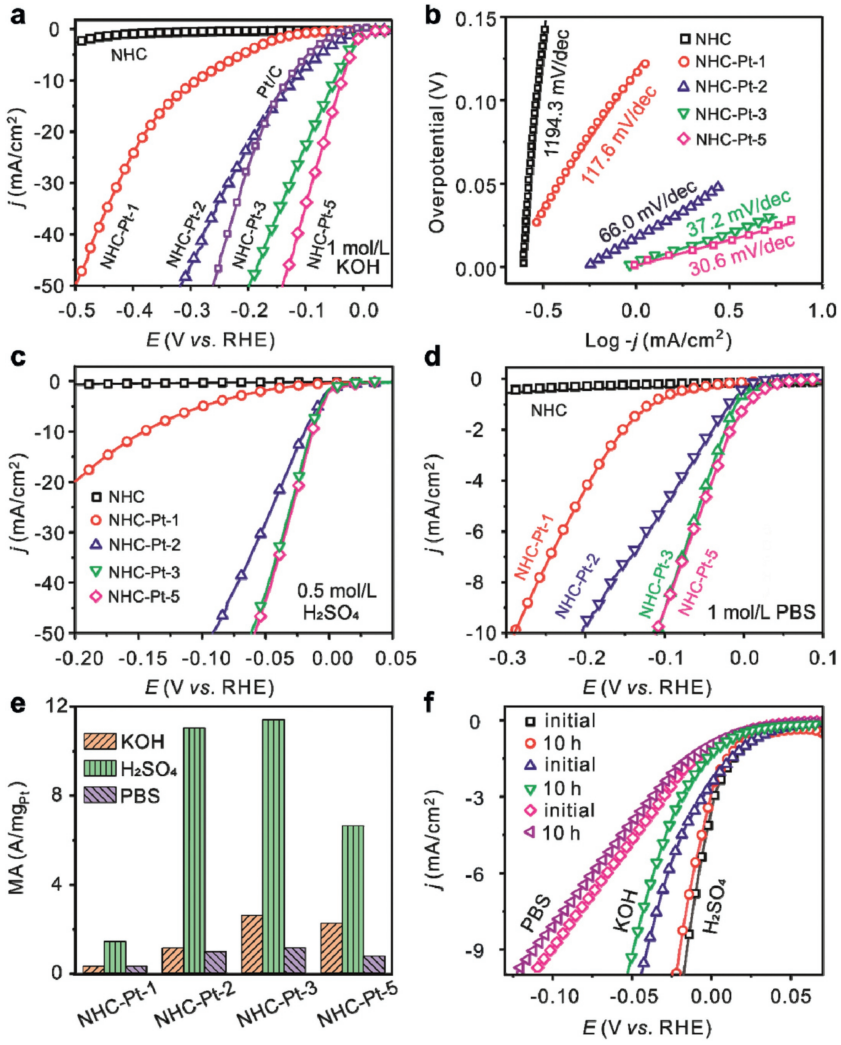

Fig. 3. Electrocatalytic performances of the catalysts for HER. (a) The linear sweep voltammetry (LSV) curves of Pt/C, NHC, NHC-Pt-1, NHC-Pt-2, NHC-Pt-3 and NHC-Pt-5 samples tested in 1 mol/L KOH. (b) The corresponding Tafel plots. LSV curves of different samples in (c) 0.5 mol/L H_2SO_4 and (d) 1 mol/L PBS solution. (e) Mass activities of NHC-Pt at overpotential of 0.05 V in KOH, H_2SO_4 and PBS solution. (f) The LSV curves of the NHC-Pt-3 sample before and after chronoamperometry test in 1 mol/L KOH, 1 mol/L PBS and 0.5 mol/L H_2SO_4 solution.

respectively (Fig. 3b), demonstrating more favorable kinetics on the NHC-Pt samples relative to the bare NHC carrier. This HER performance is comparable to the reported materials in the literature for the values of overpotentials and Tafel slopes (Table S2 in Supporting information). In 0.5 mol/L H_2SO_4 and 1 mol/L PBS electrolyte solution, the LSV curves (Figs. 3c and d) reveal that NHC is absolutely inert for HER, contrary to the fact that NHC-Pt samples exhibit much enhanced electrochemical catalytic activity in spite of the relatively low loading of Pt. The HER performance of NHC-Pt-3 is much higher than that of Pt/C in 1 mol/L KOH and 1 mol/L PBS (Fig. S7 in Supporting information). Meanwhile, Tafel plots of different samples in Figs. S8 and S9 (Supporting information) also showed that the evolvement of their value uncovers the improved catalytic kinetics with the increase of Pt loading in neutral-pH and acid media. It could be ascribed to that Pt nanoparticles serve as abundant active centers to accelerate HER kinetics and high Pt mass loading contributes to the enhanced HER activities. Furthermore, the mass activity of NHC-Pt samples normalized to the Pt loading at 0.05 V in 1 mol/L PBS, 0.5 mol/L H_2SO_4 and 1 mol/L KOH electrolytes, respectively (Fig. 3e and Fig. S10 in Supporting information). The specific activities (SA) according to the CV curves were calculated and the SA of NHC-Pt-3 is 0.494 A/m^2, which is much higher than that of Pt/C (0.287 A/m^2) at −0.1 V in 1 mol/L KOH electrolytes (Fig. S11 in Supporting information). In spite of the fact that the improvement of HER performance is in line with the increasing of Pt loadings, the mass activity of NHC-Pt-3 exceeds that of other NHC-Pt series catalysts. This indicates that the usage of Pt in the NHC-Pt-3 sample is the highest in a pH-universal solution. Furthermore, the electrical double-layered capacitance (C_{dl}) of different materials were evaluated according to the slope of the curves which plotted the $(j_a - j_c)/2$ with scan rate (j_a, anodic current density; j_c, cathodic current density). The j_a and j_c were obtained from the cyclic voltammetry (CV) curves at 0.5 V in the non-Faraday region. It can be seen from the CV curves that the current density was enhanced with the increasing of the scan rate for all the tested catalysts (Fig. S12 in Supporting information). As a result, the calculated C_{dl} data were enhanced in accordance with the Pt loading and the NHC-Pt-3 and NHC-Pt-5 showed the similar values, indicating that more exposed active sites and enhanced HER performance.

Moreover, the long-term stability test was carried out by chronoamperometry curves at the constant potential which was corresponding to the current density of 10 mA/cm^2 at LSV curves. Fig. S13 (Supporting information) showed the chronoamperometry curves of the NHC-Pt-3 composite for 10 h in KOH, H_2SO_4 and PBS solution. The current density went down at first and then main-

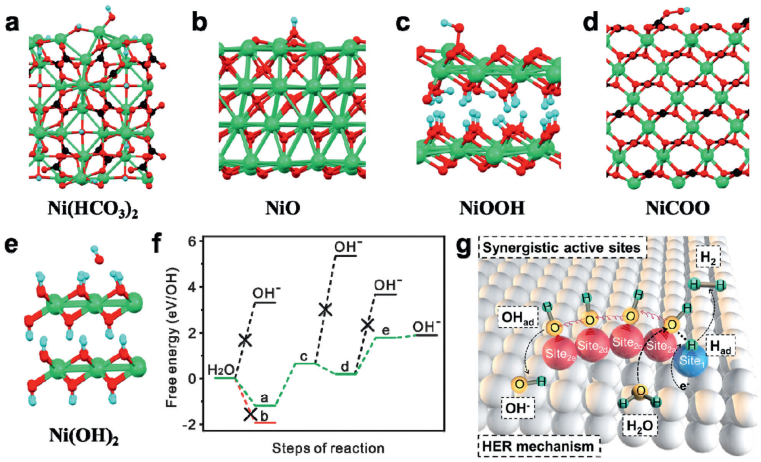

Fig. 4. Optimized atomic structure of (001) surface of $Ni(HCO_3)_2$ (a), Ni-terminated (111) surface of NiO (b), (001) surfaces of NiOOH (c), NiCOO (d) and $Ni(OH)_2$ (e) with adsorbed hydroxyl group. On panels (a-e) nickel atoms are shown in green, oxygen in red, carbon in black, and hydrogen in cyan. On the panel (f) shown free energy diagram of the adsorption (red line), desorption (black lines) and migration of hydroxyl group over considered substrates (green line, see text), the letters of panel (f) are corresponding with the structures reported on panels (a-e). (g) Schematic diagram of the possible pathways of electrocatalytic water splitting according to the DFT calculations.

tained at a certain value. The LSV curves before and after durable test were shown in Fig. 3f, where the current densities of the samples decreased slightly after 10 h of continuous reaction. The overpotentials showed slight enhancement after durable test in pH-universal environment, indicating the relatively stable of NHC-Pt-3 compound (Fig. S14 in Supporting information). The TEM images were conducted to analyze the morphological changes before and after stabilization as shown in Fig. S15 (Supporting information). It can be seen that the NHC was still retained its original structure and the size of the nanosheet is increased. The Pt nanoparticles were still distributed uniformly on NHC surface after 10 h stabilization.

The density functional theory (DFT) calculations were employed to unravel the mechanism of hydrogen production and the interaction between Pt and NHC carrier in NHC-Pt for efficient HER. For the modeling of catalytic activity of NHC-Pt co-catalyst, we take realistic structure of this material (Fig. 4a). Both XPS measurements (Fig. 2a) and the relative reference have evidenced the instability of $Ni(HCO_3)_2$ to a certain degree and reveals the presence of multiple interface areas [38,39]. These Ni-centers in different states were located and we used different Ni-based compounds to simulate these areas. In other words, a catalytic substrate can be described as a system of multiple horizontal interfaces. Thus, migration of the hydroxyl group occurs on neighboring active sites across these interfaces from the active sites of one Ni-based compound to the active site of another compound. Thus we will also consider other Ni-based structures such as Ni-terminated (111) surface of NiO (Fig. 4b), which is discussed as one decomposition product of $Ni(HCO_3)_2$, and (001) surfaces of NOOH, NiCOO and $Ni(OH)_2$ (Figs. 4c–e). Note that atomic structure of these Ni-based compounds can also be a proper model of multiple facets of $Ni(HCO)_3$ and NiOOH can also be used as a model of oxygen-terminated surface of NiO. The next step after choosing the proper model is the choosing of reaction pathways.

In contrast to the HER in acidic media where the first step is unambiguous (Eq. 1):

$$H^+ \rightarrow c\text{–}H \quad (1)$$

where "c" is notation for catalyst, in alkaline media this first step can be realized *via* three different routes (Eqs. 2a-c):

$$H_2O \rightarrow c\text{–}H + OH^- \text{ or} \quad (2a)$$

$$H_2O \rightarrow c\text{–}H + c\text{–}OH \text{ or} \quad (2b)$$

$$H_2O \rightarrow c1\text{–}H + c2\text{–}OH \quad (2c)$$

where c1 and c2 are different co-catalyst located in close proximity (Figs. 1c and d). The first route (Eq. 2a) is the least energetically favorable due to high energy cost of the formation of free OH^- group (Fig. 4f). In other steps, this energy is reduced to the intermediate adsorption of hydroxyl group on other site of the same catalyst that already interacts with hydrogen (Eq. 2b) or on other catalyst (co-catalyst, Eq. 2c). Note that the reaction shown in Eq. 2b requires simultaneous reduction and oxidation of the same catalyst and hence can be discussed only for alloys which have different active sites. Note that potential irreversible oxidation of active sites Eq. 2b can limit the performance of the catalyst over time. Resent successes in employment of co-catalyst for HER in alkaline media suggest preferred ability of the third route. In all three pathways of (Eqs. 2a–c) adsorption of hydrogen on catalyst is similar to the Volmer step of HER in acidic media (Eq. 1). Therefore, further evolution of hydrogen on Pt surface will be realized through the Heyrovsky step (Eq. 3):

$$c\text{–}H + H^+ \rightarrow H_2 \quad (3)$$

This process has been discussed in previous works and the energy cost of this step is about 0.1 eV [40,41] which is much smaller than the magnitudes of the energies corresponding with hydroxyl group (Fig. 4f and Fig. S16 in Supporting information). Hence hydroxyl related processes determine the reaction rates in HER in alkaline media.

Based on discussions above we performed calculations of the energetics of the adsorption of hydroxyl groups after water decomposition (Eq. 2c) on various substrates. These energies also determine the energy of desorption of hydroxyl groups from the substrates (Eq. 4):

$$c2\text{–}OH + e^- \rightarrow OH \quad (4)$$

In results of the calculations, we have found a large deviation of the magnitudes of desorption energies. The adsorption energy in the case of $Ni(HCO)_3$ is moderate and negative while it is also negative but with larger magnitude in the case of NiO. Thus we should rule out NiO from further consideration because adsorption of hydroxyl groups on the nickel oxide surface leads to irreversible

oxidation of the surface and formation of NOOH-like structure with Ni(III). Taking into account experimental evidences of the atomic oxygen migration over surfaces of metals, oxides and perovskites even at moderate temperatures [42–44], Eq. 4 can be rewritten as the chain of reactions (Eq. 5):

$$c2\text{–}OH \rightarrow c3\text{–}OH \rightarrow \ldots cx\text{–}OH + e^- \rightarrow OH \quad (5)$$

Eq. 5 describes a migration of hydroxyl group from one Ni-based substrate to other with the magnitude of the energy cost of the reaction much smaller than for hydroxyl group desorption until the energy cost of former process became negligible (Fig. 4f). This process of gradual migration and finally desorption of hydroxyl group with involving of all considered Ni-based systems (except NiO) can be described by further way: $Ni(HCO_3)_2\cdots OH$ (Fig. 4a) → $NiOOH\cdots OH$ (Fig. 4c) → $NiCOO\cdots OH$ (Fig. 4d) → $Ni(OH)_2\cdots OH$ (Fig. 4e)→ OH^-. The formation of the robust Ni-OH bonds leads to the favorability of the initial step of the process corresponding with Eq. 2c and step marked by letter "a" on Fig. 4f. Further formation of weaker Ni-O-OH bond requires payment of the moderate energy costs (steps marked by letter "c" and "d" on Fig. 4f) with further migration of hydroxyl group to $Ni(OH)_2$ host with formation of rather weak hydrogen bonds with Ni–OH–Ni bridges. At the last step of the process hydroxyl group desorbed from $Ni(OH)_2$ substrate is almost barrierless. Thus $Ni(OH)_2$ can be described as the final destination in the process of hydroxyl groups migration over the mix of considered Ni-based structures.

Note that the proposed three step migration process is the only pathway corresponding with involving of all considered Ni-based structure. Since the local combinations of the Ni-based structure are definitively different, the steps of migration of the hydroxyl group from $Ni(HCO_3)_2$ to $Ni(OH)_2$ is also different. However, the energy costs of each step of the migration are smaller than the energy of hydroxyl group desorption. Even in straightforward migration of the hydroxyl group from $Ni(HCO_3)_2$ to $Ni(OH)_2$ is about 0.4 eV more energetically favorable than desorption of the hydroxyl group from $Ni(HCO_3)_2$. Thus possible migration pathways can be realized in different parts of the same catalysts and the possible pathways of electrocatalytic water splitting are shown in Fig. 4g. The synergetic effect of Pt and mix of Ni-based systems found in our modeling makes possible further guided devise of composite co-catalysts for HER in alkaline media.

In conclusion, the alkaline performance improvement mechanism of HER was explored by NHC-Pt hierarchical nanostructure based on theoretical and experimental research. The NHC could affect the chemical state and electronic structure of Pt nanoparticles, which could reduce the reaction energy barriers, facilitate the adsorption of hydrogen and establish H–H bond. Moreover, DFT calculations reveal that the related process of hydroxide is the rate-determining step in the alkaline medium. The process of hydroxyl group desorption can be described as gradual migration from $Ni(HCO_3)_2\cdots OH$ directly or *via* other Ni-based systems to $Ni(OH)_2\cdots OH$ where the hydroxyl group desorbed almost barrierless. As a result, the hierarchical nanostructure of NHC-Pt-5 demonstrated an overpotential of 37 mV to achieve a current density of 10 mA/cm^2 and mass activities of 2.6 A/mg_{Pt} at 0.05 V in a 1 mol/L KOH solution. This performance could be originated from the cooperative adsorption of hydrogen and hydroxyl on NHC-Pt with synergistic active sites. This work provided a new avenue to design the hierarchical nanostructure catalysts with enhanced HER performance by constructing the synergistic active sites.

Declaration of competing interests

The authors declare that they have no conflict of interest.

CRediT authorship contribution statement

Weiping Xiao: Writing – original draft, Validation, Software, Investigation, Data curation, Conceptualization. **Yuhang Chen:** Validation, Investigation, Formal analysis. **Qin Zhao:** Software, Formal analysis. **Danil Bukhvalov:** Formal analysis, Data curation. **Caiqin Wang:** Investigation, Formal analysis. **Xiaofei Yang:** Supervision, Funding acquisition.

Acknowledgment

This work is supported from Science Fund for Distinguished Young Scholars of Nanjing Forestry University (No. JC2019002).

Supplementary materials

Supplementary material associated with this article can be found, in the online version, at doi:10.1016/j.cclet.2024.110176.

References

[1] R. Wu, J. Xu, C.L. Zhao, et al., Nat. Commun. 14 (2023) 2306.
[2] L. Yang, R. Grzeschik, P. Jiang, et al., Angew. Chem. Int. Ed. 62 (2023) 202302126.
[3] Y. Zhu, K. Fan, C.S. Hsu, et al., Adv. Mater. 35 (2023) 2301133.
[4] Q. Li, Y. Gao, M. Liu, et al., J. Colloid Interface Sci. 646 (2023) 391–398.
[5] Y. Lai, Z. Zhang, Z. Zhang, et al., Chem. Eng. J. 435 (2022) 135102.
[6] K. Liu, H. Yang, Y. Jiang, et al., Nat. Commun. 14 (2023) 2424.
[7] M. Cococcioni, S. de Gironcoli, Phys. Rev. B 71 (2005) 035105.
[8] Z. Wu, P. Yang, Q. Li, et al., Angew. Chem. Int. Ed. 62 (2023) 202300406.
[9] P. Wang, Y. Yan, P. Wang, et al., Chem. Eng. J. 455 (2023) 140856.
[10] J. Durst, A. Siebel, C. Simon, et al., Energy Environ. Sci. 7 (2014) 2255–2260.
[11] T.J. Schmidt, P.N. Ross, N.M. Markovic, J. Electroanal. Chem. 524–525 (2002) 252–260.
[12] W. Sheng, M. Myint, J.G. Chen, Y. Yan, Energy Environ. Sci. 6 (2013) 1509–1512.
[13] F. Li, G.F. Han, H.J. Noh, et al., Nat. Commun. 10 (2019) 4060.
[14] W. Sheng, Z. Zhuang, M. Gao, et al., Nat. Commun. 6 (2015) 5848.
[15] J. Zheng, W. Sheng, Z. Zhuang, B. Xu, Y. Yan, Sci. Adv. 2 (2016) 1501602.
[16] K. Elbert, J. Hu, Z. Ma, et al., ACS Catal. 5 (2015) 6764–6772.
[17] S. Xu, M. Niu, G. Zhao, et al., Nano Res. 16 (2023) 6212–6219.
[18] S. Lu, Z. Zhuang, J. Am. Chem. Soc. 139 (2017) 5156–5163.
[19] Y. Wang, G. Wang, G. Li, et al., Energy Environ. Sci. 8 (2014) 177–181.
[20] L. Wang, H.N. Liu, X. Meng, et al., Rare Met. 43 (2024) 2851–2858.
[21] J. Dai, Y. Zhu, H.A. Tahini, Nat. Commun. 11 (2020) 5657.
[22] I.T. McCrum, M.T.M. Koper, Nat. Energy 5 (2020) 891–899.
[23] R. Subbaraman, D. Tripkovic, D. Strmcnik, et al., Science 334 (2011) 1256–1260.
[24] E. Liu, J. Li, L. Jiao, et al., J. Am. Chem. Soc. 141 (2019) 3232–3239.
[25] D. Strmcnik, M. Uchimura, C. Wang, et al., Nat. Chem. 5 (2013) 300–306.
[26] M.Y. Fan, J.J. Wang, J. Zhao, et al., Rare Met. 43 (2024) 1537–1546.
[27] B. Zhou, Y. Li, Y. Zou, et al., Angew. Chem. Int. Ed. 60 (2021) 22908–22914.
[28] V.R. Stamenkovic, B.S. Mun, M. Arenz, et al., Nat. Mater. 6 (2007) 241–247.
[29] H. Yin, S. Zhao, K. Zhao, et al., Nat. Commun. 6 (2015) 6430.
[30] Y. Wei, G. Cheng, J. Xiong, et al., ACS Sustain. Chem. Eng. 5 (2017) 5027–5038.
[31] S. Zhao, Z. Wang, Y. He, et al., ACS Energy Lett. 2 (2017) 111–116.
[32] M. Lao, K. Rui, G. Zhao, et al., Angew. Chem. Int. Ed. 131 (2019) 5489–5491.
[33] B. Muthukutty, T.C. Doan, H. Yoo, Environ. Res. 241 (2024) 117655.
[34] K.L. Zhou, C. Wang, Z. Wang, et al., Energy Environ. Sci. 13 (2020) 3082–3092.
[35] B. Pang, X. Liu, T. Liu, et al., Energy Environ. Sci. 15 (2022) 102–108.
[36] J. Zhang, Y. Zhao, X. Guo, et al., Nat. Catal. 1 (2018) 985–992.
[37] C. Li, Z. Chen, H. Yi, et al., Angew. Chem. Int. Ed. 59 (2020) 15902–15907.
[38] Y. Dong, Y. Ma, D. Li, et al., Chem. Sci. 9 (2018) 8682–8691.
[39] C. Rincke, S. Bette, R.E. Dinnebier, W. Voigt, Eur. J. Inorg. Chem. 2015 (2015) 5913–5920.
[40] J. Greeley, T.F. Jaramillo, J. Bonde, I. Chorkendorff, J.K. Nørskov, Nat. Mater. 5 (2006) 909–913.
[41] Y. Tang, B.L. Allen, D.R. Kauffman, A. Star, J. Am. Chem. Soc. 131 (2009) 13200–13201.
[42] C. Descorme, D. Duprez, Appl. Catal. A: Gen. 202 (2000) 231–241.
[43] M. Colin, D. Duprez, M. Pélissier, Stud. Surf. Sci. Catal. 112 (1997) 303–312.
[44] L. Cao, O. Petracic, X.K. Wei, Small 17 (2021) 2104356.